

Supporting Information

Interfacial defect healing of In₂S₃/Sb₂(S,Se)₃ heterojunction solar cells with a novel wide-bandgap InOCl passivator

Changxue Wang,^{1,2} Dongdong Li,³ Xiaoli Mao,² Lei Wan,¹ Zhen Cheng,¹ Jun Zhu,⁴ Robert L. Z. Hoye,⁵ and Ru Zhou^{*,1,5}

¹ School of Electrical Engineering and Automation, Hefei University of Technology, Hefei 230009, P. R. China

² School of Microelectronics, Hefei University of Technology, Hefei 230009, P. R. China

³ School of Materials Science and Engineering, Hefei University of Technology, Hefei 230009, P. R. China

⁴ Academy of OptoElectric Technology, Hefei University of Technology, Hefei 230009, P. R. China

⁵ Inorganic Chemistry Laboratory, Department of Chemistry, University of Oxford, South Parks Road, Oxford OX1 3QR, United Kingdom

* Corresponding author:

zhouru@hfut.edu.cn (Ru Zhou)

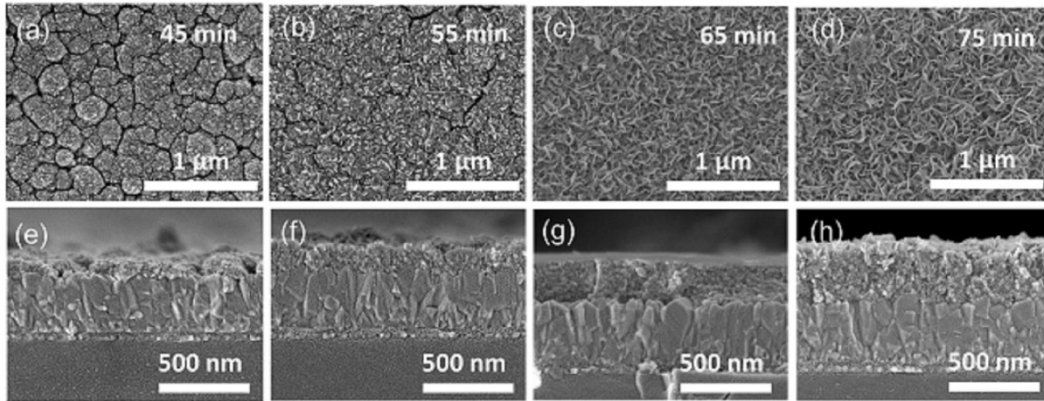


Figure S1. Top-view (a-d) and cross-sectional (e-h) SEM images of In_2S_3 deposited upon the FTO substrate under the CBD duration of 45 to 55, 65, and 75 min.

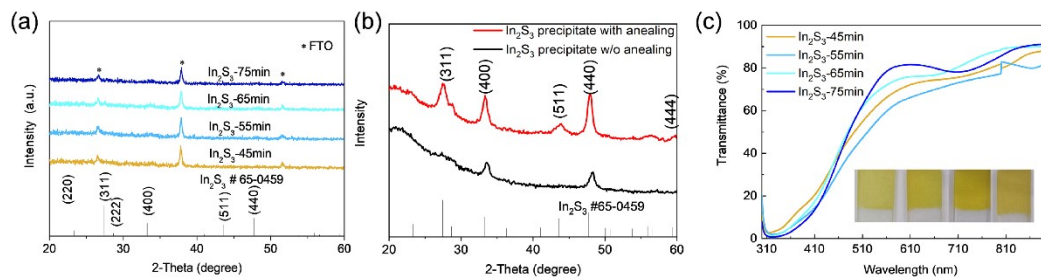


Figure S2. (a) XRD patterns of In_2S_3 films deposited on the FTO substrate under different CBD time, (b) XRD patterns of the In_2S_3 precipitates during the CBD process collected from the beaker, and (c) The transmittance spectra of In_2S_3 films processed under different CBD durations.

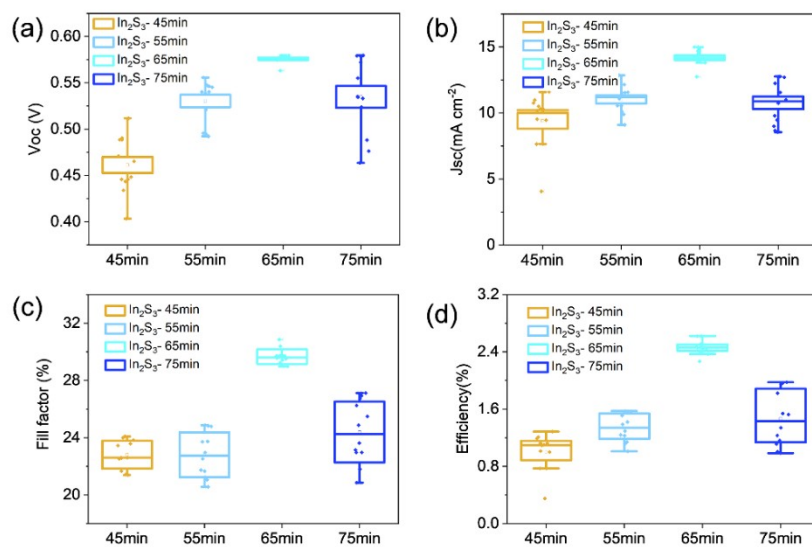


Figure S3. Box charts of device photovoltaic parameters, including (a) V_{oc} , (b) J_{sc} , (c) FF and (d) PCE, measured under the illumination of One Sun, each based on 12 pieces of devices.

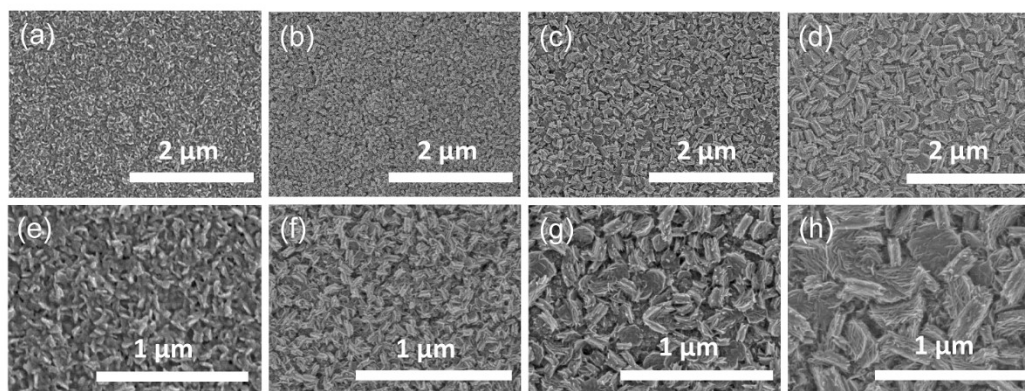


Figure S4. Top-view SEM images of In_2S_3 films processed by the InCl_3 post-treatment with the InCl_3 concentration of (a, e) 0.01, (b, f) 0.02, (c, g) 0.04, and (d, h) 0.08 g/mL.

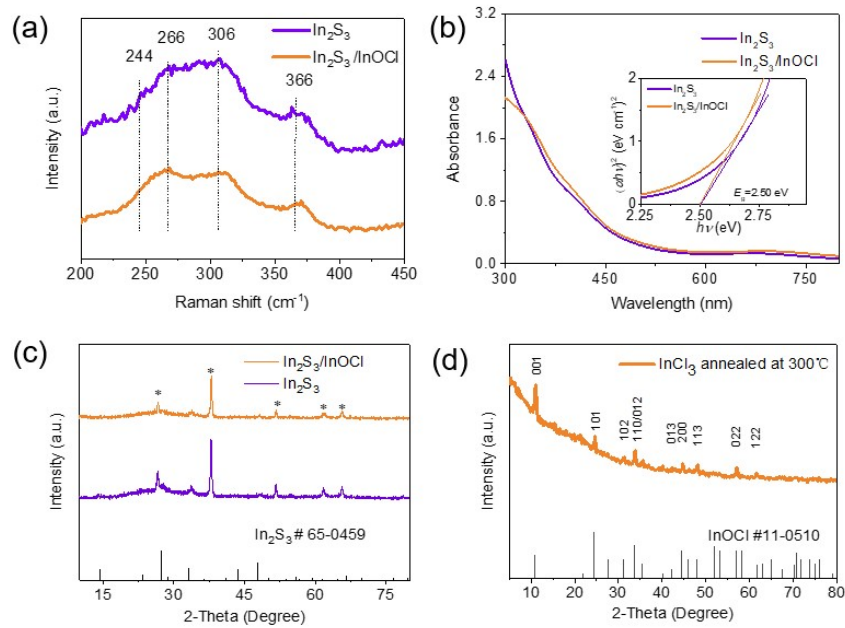


Figure S5. (a) Raman spectra of In₂S₃ films without and with InCl₃ post-treatment, performed by using 532 nm laser as the excitation source. The peaks at 244 and 306 cm⁻¹ can be assigned to the Raman-active vibrational mode of InS₆ octahedra and InS₄ tetrahedra, respectively. (b) Absorption spectra (the inset gives corresponding Tauc plots) and (c) XRD patterns of In₂S₃ films without and with the InCl₃ post-treatment. (d) XRD pattern of power samples prepared by drying the InCl₃ methanol precursor solution and further annealing at 300 °C in the Muffle furnace for 30 min.

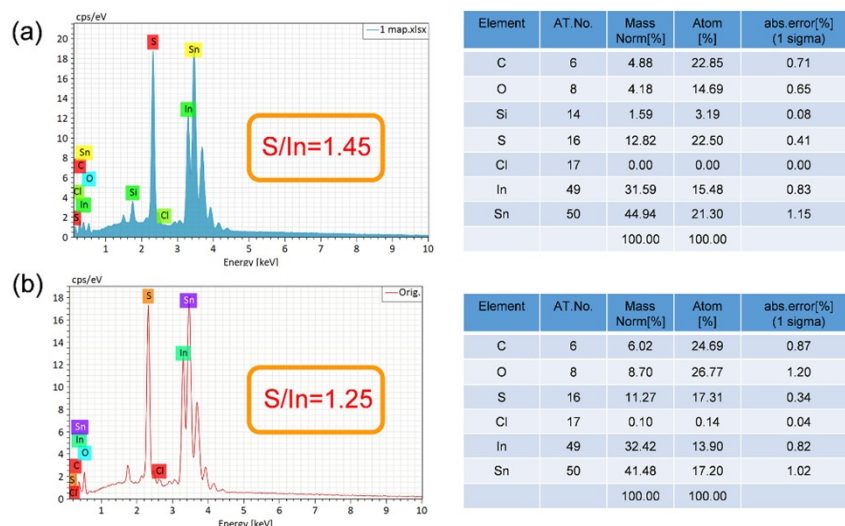


Figure S6. The EDS spectra of In₂S₃ films without (a) and with (b) the InCl₃ post-treatment, and corresponding element ratios of buffer layers.

Supplementary Note 1

Surface structural modeling of InOCl/ β -In₂S₃ (110) interface is divided into three regions, that is, the vacuum region, the surface region, and the substrate region. The surface region is simulated by a slab with a monolayer InOCl within a 2×2 surface supercell. The substrate is simulated by β -In₂S₃ (110) surface, whose cell parameter are a=b=7.909Å. The three 4-fold In vacancies are embedded into the substrate as shown in Figure S7a.

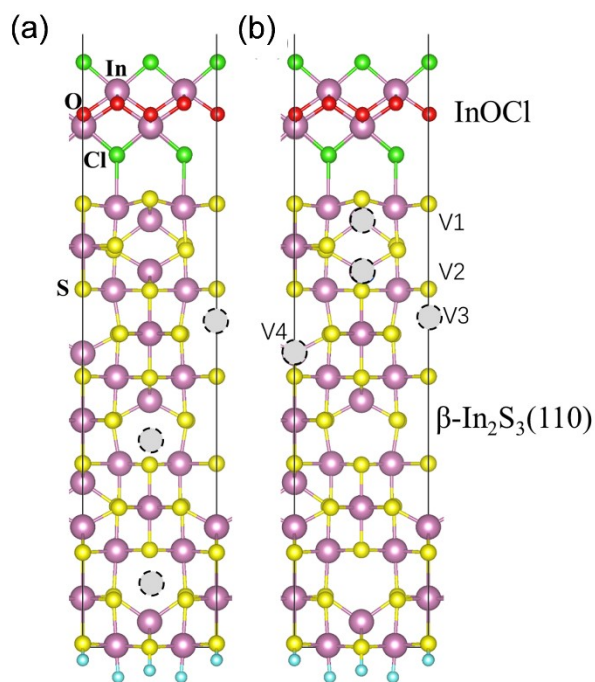


Figure S7. (a) Surface structural modeling of InOCl/ β -In₂S₃ (110) interface after structural relaxation. The three gray ball represent the 4-fold In vacancies. (b) The structural modeling of tetrahedrally coordinated In vacancies in β -In₂S₃ (110).

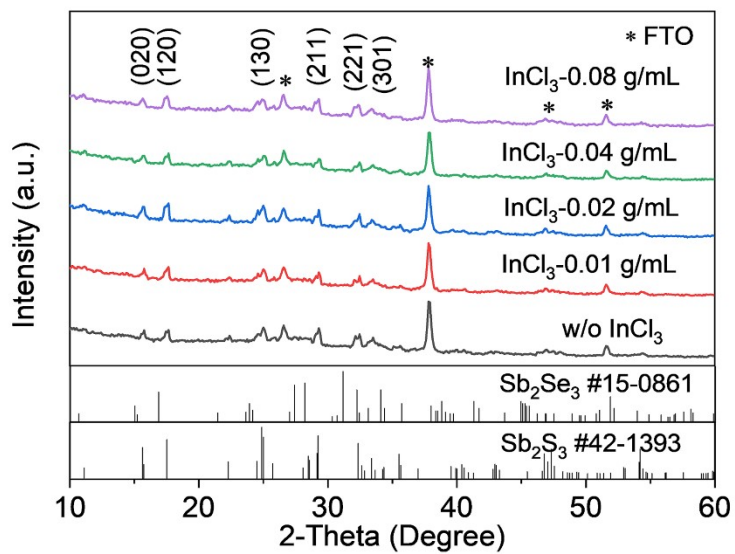


Figure S8. XRD patterns of $\text{Sb}_2(\text{S,Se})_3$ films deposited upon In_2S_3 and $\text{In}_2\text{S}_3/\text{InOCl}$ buffer layers.

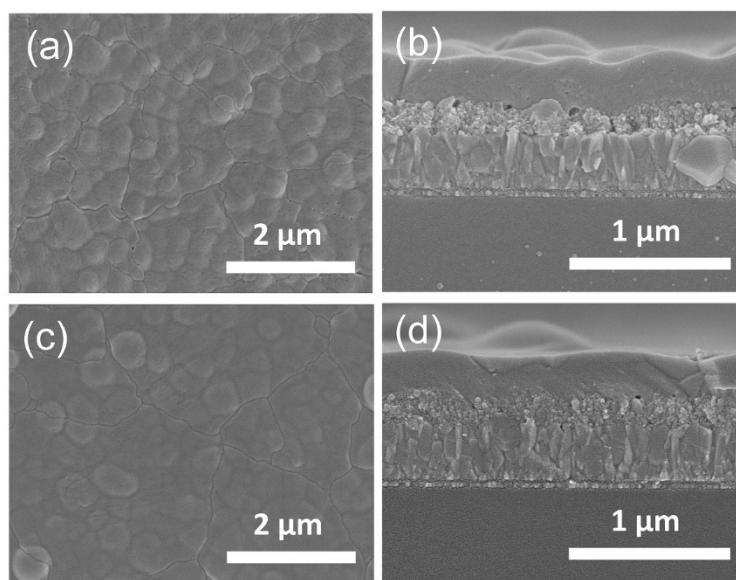


Figure S9. Top-view and cross-sectional view SEM images of $\text{Sb}_2(\text{S,Se})_3$ absorber films constructed on (a, b) In_2S_3 and (c, d) $\text{In}_2\text{S}_3/\text{InOCl}$ buffer layers.

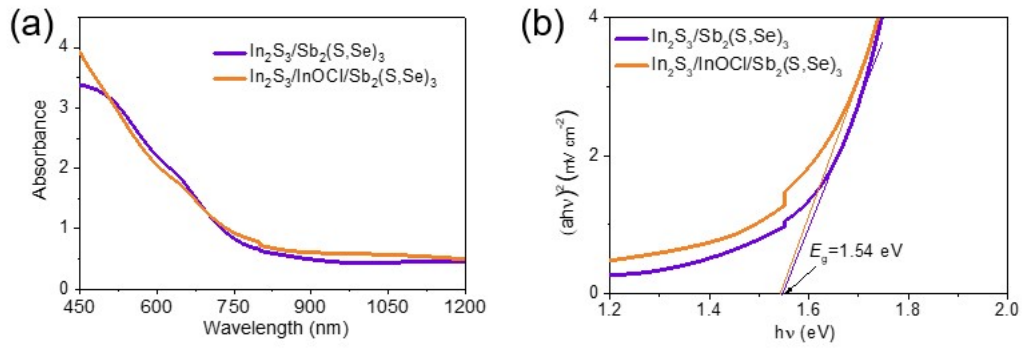


Figure S10. The absorption spectra of $\text{Sb}_2(\text{S,Se})_3$ films deposited on In_2S_3 and $\text{In}_2\text{S}_3/\text{InOCl}$ layers and corresponding Tauc plots.

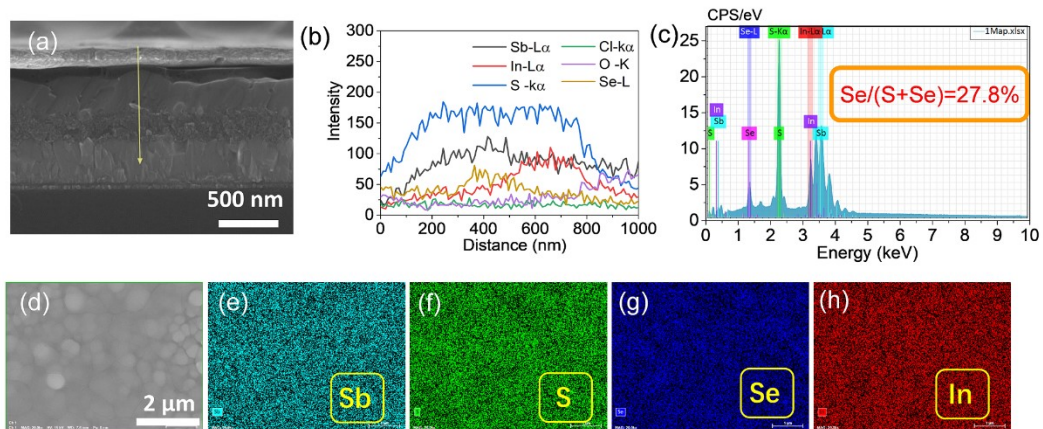


Figure S11. (a, b) The cross-sectional EDS line scan of $\text{Sb}_2(\text{S,Se})_3$ solar cells, (c) the surface EDS characterization of $\text{FTO}/\text{In}_2\text{S}_3/\text{Sb}_2(\text{S,Se})_3$ sample, and (d-h) the elemental mapping images of Sb, S, Se, and In.

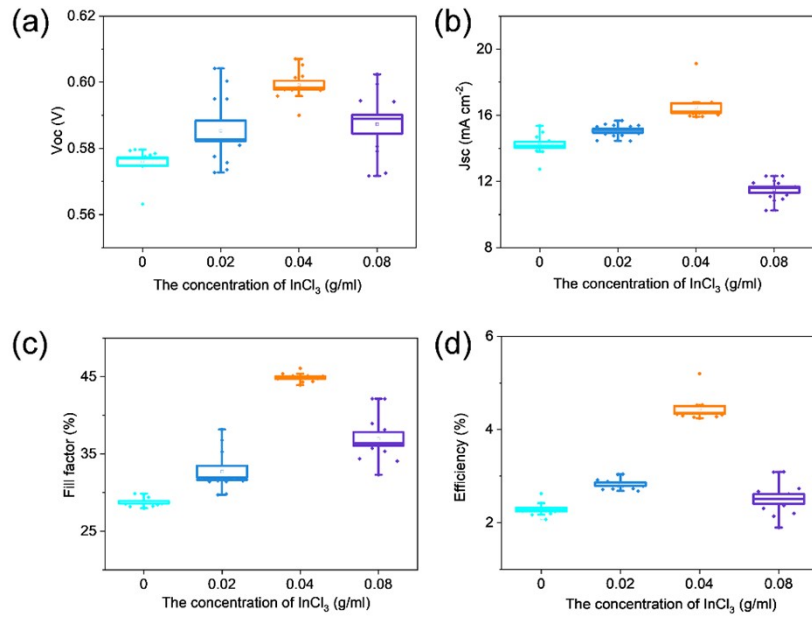


Figure S12. The box charts of performance parameters for $\text{Sb}_2(\text{S,Se})_3$ solar cells based on In_2S_3 buffer layers treated with different InCl_3 concentrations.

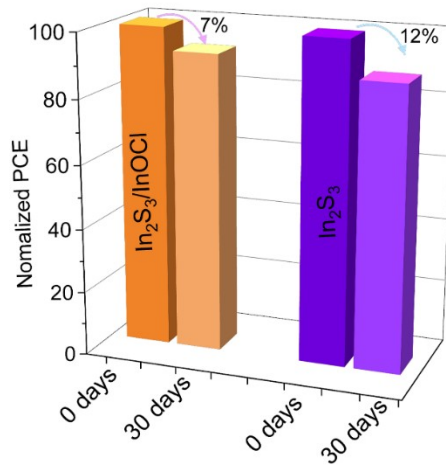


Figure S13. The device stability measurements of unencapsulated $\text{Sb}_2(\text{S,Se})_3$ solar cells placed in an electronic moisture-proof cabinet with 5% humidity.

Supplementary Note 2

UPS analysis of InOCl:

According to the intersection of the tangent line and the coordinate axis in Figure S13, the cut-off binding energy ($E_{\text{cut-off}}$) value of InOCl is 17.44 eV. According to Equation S1:

$$WF = E_{\text{cut-off}} - 21.22 \quad (\text{S1})$$

where the work function (WF) values relative to the Fermi level of InOCl is -3.78 eV. The VBM relative to the Fermi level of InOCl is estimated to be 3.81 eV. Therefore, the VBM (E_{VB}) relative to the vacuum level is calculated to be -7.59 eV, according to Equation S2:

$$E_{\text{VB}} = WF - E_{F,\text{edge}} \quad (\text{S2})$$

Combined with the bandgap of 4.07 eV, the CBM relative to the vacuum level of InOCl is -3.52 eV.

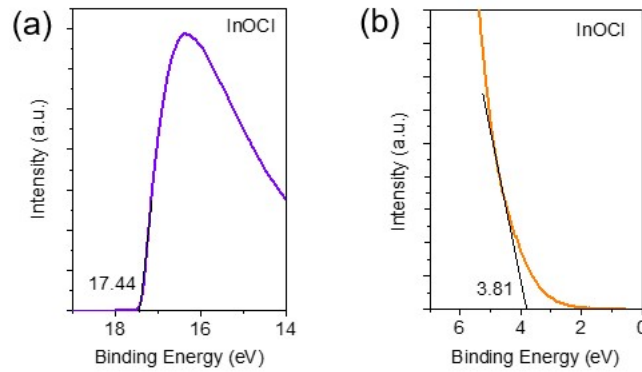


Figure S14. UPS spectra of InOCl film (a) at the secondary electron cut-off and (b) near the Fermi edge.

Supplementary Note 3

The unit cell of InOCl displays an orthorhombic lattice with a space group of Pmmn. The optimized cell parameter a and b of InOCl monolayer are 3.575 and 4.154, respectively. In electronic structural calculations, $3 \times 3 \times 1$ Monkhorst Pack k-point set was used for HSE06 self-consistent calculation and for DOS calculation of InOCl. In HSE06, standard parameters: $\alpha = 0.25$ and $w = 0.20$ were used, which work well for correcting the band gaps of common semiconductors. It turns out that the band gap of InOCl presents an indirect nature and the direct band gap is estimated to be 4.07 eV.

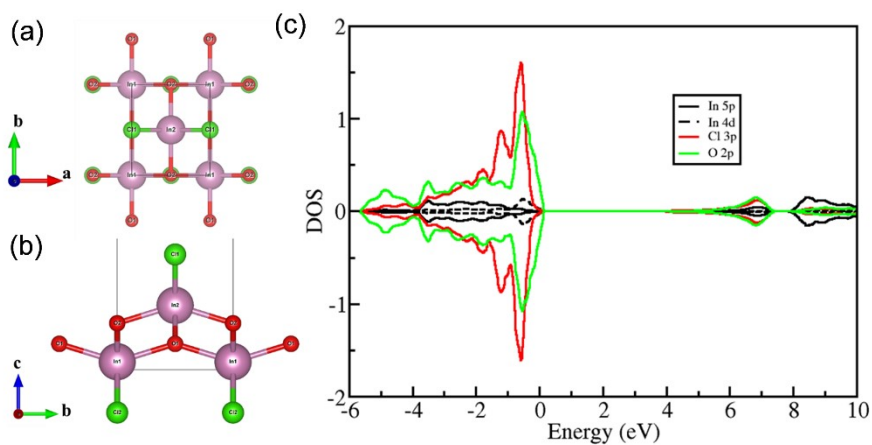


Figure S15. (a) Top view and (b) side view of the structure of InOCl monolayer, and (c) DOS of In, O and Cl atoms.

Table S1 The comparison of material, optical, electric properties between In_2S_3 and other commonly used ETLs

ETL	Toxicity	Processing temperature (°C)	Compatibility with flexible substrate	Carrier mobility ($\text{cm}^2 \text{V}^{-1} \text{s}^{-1}$)	Bandgap (eV)	Carrier concentration (cm^{-3})
CdS	Yes	400	moderate	4.66	2.4	10^{16}
TiO_2	No	450-500	No	<1	3.0-3.2	10^{17}
ZnO	No	350-450	moderate	300	3.2	10^{18}
SnO_2	No	~450	moderate	240	3.6	10^{15}
Zn(O,S)	No	~400	moderate	/	2.6-3.8	/
In_2S_3	No	300	Excellent	17.6	2.2-2.8	10^{12}

Table S2 The impedance fitting results of $\text{Sb}_2(\text{S,Se})_3$ solar cells based on In_2S_3 and $\text{In}_2\text{S}_3/\text{InOCl}$ buffer layers

Devices	R_{ser} (Ω)	R_{rec} ($\text{k}\Omega$)	CPE-T (F)	CPE-P (F)
In_2S_3	13.2	16.72	3.51×10^{-9}	0.99
$\text{In}_2\text{S}_3/\text{InOCl}$	17.6	27.28	1.94×10^{-8}	0.92